A Photo-Crosslinkable Bis-Triarylamine Side-Chain Polymer as a Hole-Transport Material for Stable Perovskite Solar Cells

Marie-Hélène Tremblay,‡[a] Kelly Schutt,‡[b] Yadong Zhang,[a] Jongchul Lim[b], Jonathan H. Warby[b], Yen-Hung Lin[b], Stephen Barlow[a], Henry J. Snaith[b], and Seth R. Marder[a*]

[a.] School of Chemistry and Biochemistry, and Center for Organic Photonics and Electronics (COPE), Georgia Institute of Technology GA, Atlanta 30332-0400, United States
[b.] Clarendon Laboratory, Department of Physics, University of Oxford, Parks Road, Oxford OX1 3PU, United Kingdom See DOI:

‡ Authors contributed equally to the manuscript.

*Corresponding author: Seth R. Marder, seth.marder@chemistry.gatech.edu

Supporting information

Table of contents

1. Experimental Procedures

Synthesis. P1-2 was synthesized according to the literature.[1]

CL1-2. **P1-2** was crosslinked after the thermal annealing step under ambient atmosphere by using a UV lamp with an emission maximum at 356 nm. The sample was placed 5.5 cm from the lamp, at which distance the UV-light intensity was 17.5 mW cm^{-2}, for 4 min. We note that the thermal annealing at 130 °C does not result in any significant crosslinking, as evidenced by UV-vis absorption spectroscopy (which shows no change in the absorbance at ca. 310 nm, to which cinnamate contributes) and by the solvent resistance of the film.

UV−Vis absorption spectroscopy. Absorbance spectra were measured with a Cary 5000 UV−vis/NIR spectrometer. For liquid measurement, the samples were dissolved in anhydrous and degassed toluene. For solid-state measurement, the samples were prepared by spincoating the HTM on glass substrates.

Fluorescence spectroscopy. Fluorescence spectra were measured with a Horiba Jobin Yvon Fluorolog 3-2i spectrometer.

Cyclic voltammetry (CV). Cyclic voltammetry experiments were performed using a BAS potentiostat with a glassy carbon working electrode, platinum counter electrode and an Ag wire reference electrode at a scan rate of 100 mV s^{-1}. Anhydrous and degassed dichloromethane solutions containing 0.1 M of tetrabutylammonium hexafluorophosphate as electrolyte was used to dissolve **1** (10^{-3} M). Ferrocene was used as the reference.

Current−voltage measurements. The *JV* curves were measured (2400 Series SourceMeter, Keithley Instruments) under simulated AM 1.5 sunlight at 100 mW cm^{-2} irradiance generated by an Abet Class AAB sun 2000 simulator, with the intensity calibrated with an NREL calibrated KG 5 filtered Si reference cell. The forward *J–V* scans were measured from forward bias to short circuit and the backward scans were from short circuit to forward bias, both at a scan rate of 380 mV s^{-1}. A stabilization time of 5 s at forward bias of 0 V under illumination was done prior to scanning.

Scanning electron microscope. SEM images were measured using a FEI Sirion scanning electron microscope at an acceleration voltage of 5 kV.

Powder X-ray diffraction. XRD spectra were measured using a Panalytical X'pert powder diffractometer with Cu anode X-ray source.

Conductivity. Conductivity data were acquired with a custom built 4 point probe system with Au contact pins connected to a Keithly 2636 SourceMeter. To prepare the substrates, X nm of gold was evaporated on clean glass substrates and the HTM was spincoated from a toluene solution.

Profilometry. Film thicknesses were measured with a Veeco Dektak 150 surface profilometer.

AFM. Atomic force microscopy images were acquired with an Asylum MFP3D (Asylum Research and Oxford Instruments Co.) in AC (tapping) mode. Asylum Research Econo-LTESP-Au silicon tips were used for topography measurements.

Substrate preparation. Fluorine doped tin oxide (FTO) (Pilkington TEC 7) or indium tin oxides (ITO) (Shenzhen Display, < 10 ohm cm^{-2}) coated glass substrates were used in this experiment. FTO or ITO substrates were etched at specific regions using a 2 M HCl and zinc powder. Substrates were then cleaned with water, then sequentially sonicated for 5 min in acetone, isopropyl alcohol and water, and dried with a compressed nitrogen gun. Next, the substrates were treated for 5 min in oxygen plasma.

F_4-TCNQ-doped PolyTPD. 0.2 mg of F_4-TCNQ and 1 mg of PolyTPD were added to 1 mL of toluene. The solution was stirred for 12 h prior to deposition. The filtered solution was spincoated at 2000 rpm, 2000 rpm s^{-1} for 20 s and dried at 130 °C for 10 min. PFN (9,9-bis(3-(*N,N*-dimethylamino)propyl)fluorene-2,7-diyl)-*alt*-(9,9-dioctylfluoren-2,7-diyl) devices were made by spin coating 0.1 mg mL^{-1} PFN in methanol onto the annealed PolyTPD substrate at 3000 rpm for 30 s.

F_4-TCNQ-doped P1-2. For undoped films, 1 mg of **P1-2** was added to 1 mL of toluene. The solution was stirred for 12 h prior to deposition. The filtered solution was spincoated at 2000 rpm, 2000 rpm s^{-1} for 20 s and dried at 130 °C for 10 min. For doped films, a solution of 0.5 mg mL^{-1} of F_4-TCNQ in toluene was added to **P1-2** solution in toluene (2 mg mL^{-1}) at the mol% desired and toluene was added to achieve a 1 mg mL^{-1} solution of **P1-2**.

$Cs_{0.05}(FA_{0.85}MA_{0.15})_{0.95}Pb(I_{0.9}Br_{0.1})_3$ perovskite (FAMACs). The precursor solution was prepared by dissolving formamidinium iodide (FAI; Dyesol), methylammonium iodide (MAI; Dyesol), cesium iodide (CsI; Sigma Aldrich), lead iodide (PbI_2; TCI) and lead bromide ($PbBr_2$; Alfa Aesar) in anhydrous *N,N*-dimethylformamide (DMF; Sigma-Aldrich) and dimethylsulfoxide (DMSO; Sigma-Aldrich) in a ratio 4:1 in a nitrogen-filled glovebox to obtain a stoichiometric 1.3 M solution. The solution was then stirred overnight at room temperature and filtered using a 0.44 μm filter. 150 μL of the precursor perovskite solution was spin-coated in a drybox at 1000 rpm for 10 s and then 6000 rpm for 35 s with a ramp of 2000 rpm s^{-1}. After 35 s, 400 μL of toluene (Sigma) was quickly added on the spinning substrates. The films were dried on a hot plate at a temperature of 100 °C for 60 min.

$FA_{0.83}Cs_{0.17}Pb(I_{0.83}Br_{0.17})_3$ perovskite (FACs). A 1.45 M solution was stirred at 70 °C for 15 min immediately prior to use. 64.0 mg CsI, 103.8 mg $PbBr_2$, 207.0 mg FAI, and 538.2 mg PbI_2 were added to 800 μL DMF and 200 μL DMSO. The solution was then stirred overnight at room temperature. 150 μL of the precursor perovskite solution was spin-coated in a drybox at 1000 rpm for 10 s and then 6000 rpm for 35 s with a ramp of 2000 rpm s^{-1}. After 30 s, 400 μL of toluene (Sigma) was quickly added on the spinning substrates. The films were dried on a hot plate at a temperature of 100 °C for 60 min.

Electron-transport material. PCBM (PCBM = phenyl-C_{61}-butyric acid methyl ester) (20 mg mL^{-1} in 3:1 chlorobenzene/dichlorobenzene) and BCP (BCP = bathocuproine) (0.5 mg mL^{-1} in isopropanol) were stirred overnight prior to deposition. They were then sequentially dynamically deposited by spin coating. First, PCBM was deposited at 2000 rpm for 20 s, followed by annealing for 5 min at 100 °C. Second, BCP was deposited at 5000 rpm for 20 s followed by annealing at 100 °C for 1 min.

Electrode evaporation. An 100 nm silver or 80 nm gold electrode was thermally evaporated under vacuum.

PL data treatment. Each normalized PL decay was fitted to a stretched exponential function following the method of Stranks *et al*.:[2]

$$I(t) = exp\left[-\left(\frac{t - t_0}{\tau}\right)^{\beta}\right]$$

with I(t) the PL intensity at time t, t_0 an offset correction (constrained such that $0 \leq t0 \leq 10$), τ the characteristic lifetime and β the stretching exponent. The use of a stretched exponential function to fit PL data from perovskite films is well established in the literature, in lieu of a true analytical model.[3,4] The stretching of the exponential has been interpreted as resulting from a distribution of monomolecular (trap-assisted) non-radiative decay rates within the material.[5] The mean relaxation time, $\langle\tau\rangle$, given by Equation 4:

$$\langle\tau\rangle = \frac{\tau}{\beta}\Gamma\left(\frac{1}{\beta}\right)$$

where Γ(z) is the gamma function:

$$\Gamma(z) = \int_0^{\infty} x^{z-1}e^{-x}dx$$

Tandem perovskite/HTM/perovskite structures. FTO substrates were cleaned as above. FACs perovskite was spin coated, then annealed at 100 °C as previously described. PolyTPD (10 mg/ml) and **P1-2** (10 mg/ml) were filtered through a 0.22 um PTFE syringe filter, then spin-

coated on top of the perovskite (2k rpm, 20 s) and annealed at 130 °C for 10 mins for layer thicknesses of approximately 68 and 50 nm, respectively. **P1-2** was then crosslinked as above. For the top layer of perovskite, $MAPbI_3$ was prepared in acetonitrile by adding PbI_2 (1.466 g) and methylammonium iodide (0.477 g) to acetonitrile (6 ml), and then bubbling the solution with methylamine for about 5 min until the solution turned from black and opaque to colorless and transparent (see ref 6 for details). Solution was dynamically dispensed onto substrates spinning at 2000 rpm for 35 s. Substrates were then annealed at 100 °C for 10 minutes. Absorption spectra were collected with a Varian Cary 1050 UV Vis spectrophotometer before thermally evaporating 80 nm of Au to improve contrast for the SEM cross section. Cross sectional images were acquired with an FEI Quanta 600 scanning electron microscope at 10 kV acceleration voltage.

2. Characterization of HTM and perovskite growth

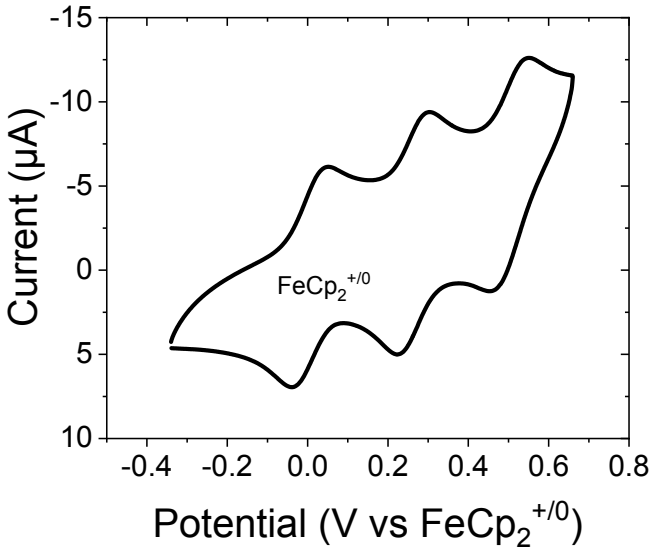

Fig. S1 Cyclic voltammetry of **1** in dichloromethane (10^{-3} M) with 0.1 M Bu_4NPF_6 and ferrocene as reference (10^{-3} M).

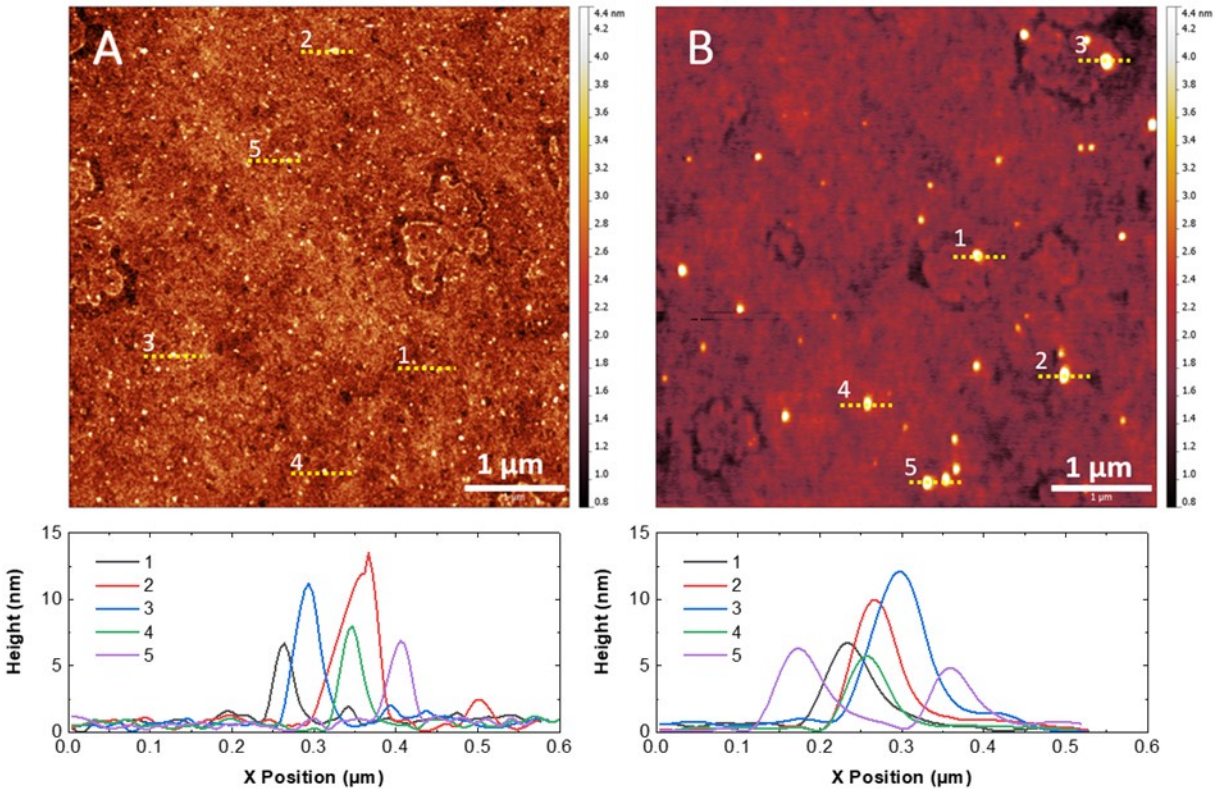

Fig. S2 – AFM images of (A) PolyTPD and (B) **CL1-2** spincoated on glass. Height profiles of surface aggregates are shown below.

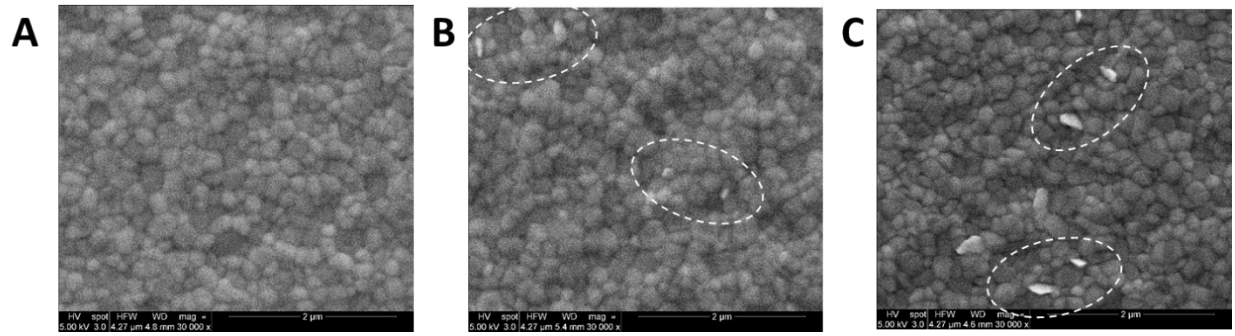

Fig. S3 SEM images of the FAMACs perovskite film crystallized on top of FTO/HTM layer, where HTM is (A) doped PolyTPD, (B) pristine **CL1-2** and (C) doped **CL1-2**. The circled bright particles are assumed to be PbI_2 crystals.

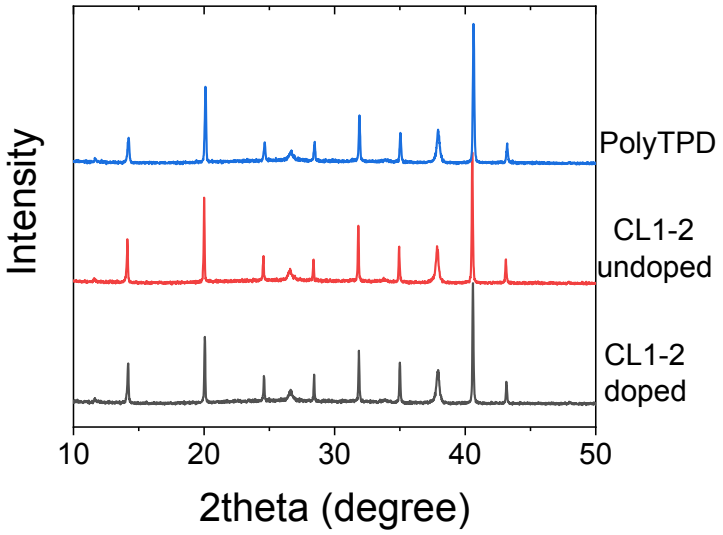

Fig. S4 PXRD of the FAMACs perovskite spincoated on PolyTPD, and doped and undoped **CL1-2** films on FTO.

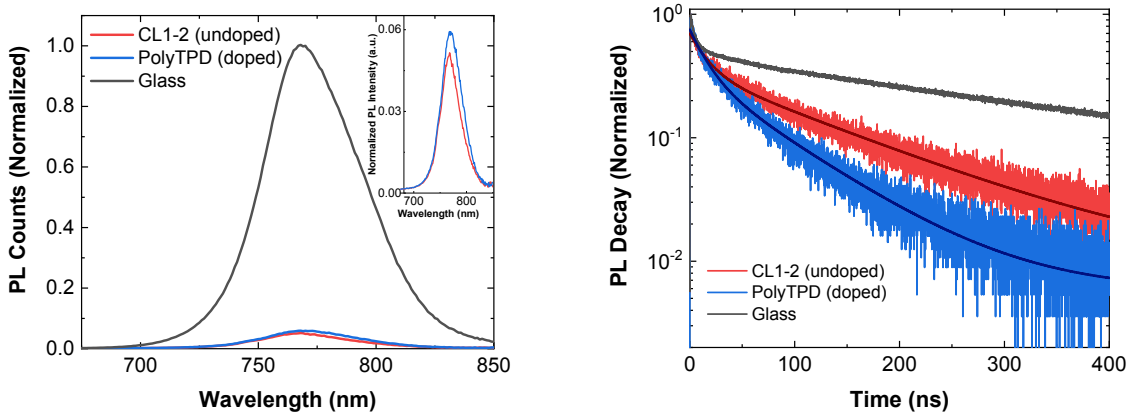

Fig. S5 Top: Photoluminescence (PL) of the FAMACs perovskite spincoated on the HTM films and on clean glass, showing similar levels of steady state photoluminescence (PL) quenching for both FTO/**CL1-2**/perovskite and FTO/PolyTPD/perovskite. The PL maximum for the PolyTPD sample is slightly red-shifted (770 nm) relative to the **CL1-2** and the perovskite-on-glass sample (both 768 nm), which may indicate more band-bending due to shallow-trap formation in the PolyTPD case.[7,8] Bottom: Time-resolved PL of the FAMACs perovskite spincoated on the HTM (doped PolyTPD, undoped **CL1-2**) films and on glass. Fitting as a biexponential decay

$$Y = A_1 \exp\left(\frac{-t}{\tau_1}\right) + A_1 \exp\left(\frac{-t}{\tau_2}\right) + y_0$$

where τ_1 is the lifetime for fast, trap-assisted processes (Shockley-Read-Hall recombination), τ_2 is the lifetime for slower bimolecular recombination, and A_1 and A_2 are the relative amplitudes,[9] gave lifetimes τ_1 = 16.1 ns and τ_2 = 127.5 ns for the **CL-2** sample, while the perovskite film on doped PolyTPD exhibits

lifetimes of τ_1 = 15.7 ns and a reduced τ_2 lifetime of 74.5 ns. In contrast, the perovskite on glass, where bulk recombination processes dominate, exhibits a much longer τ_2 lifetime of 324.2 ns.

3. Additional device characterization

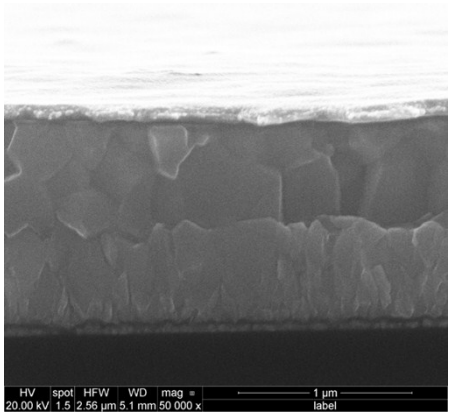

Fig. S6 SEM image of device cross-section for FTO/PolyTPD/FAMACs/PCBM/BCP/Ag.

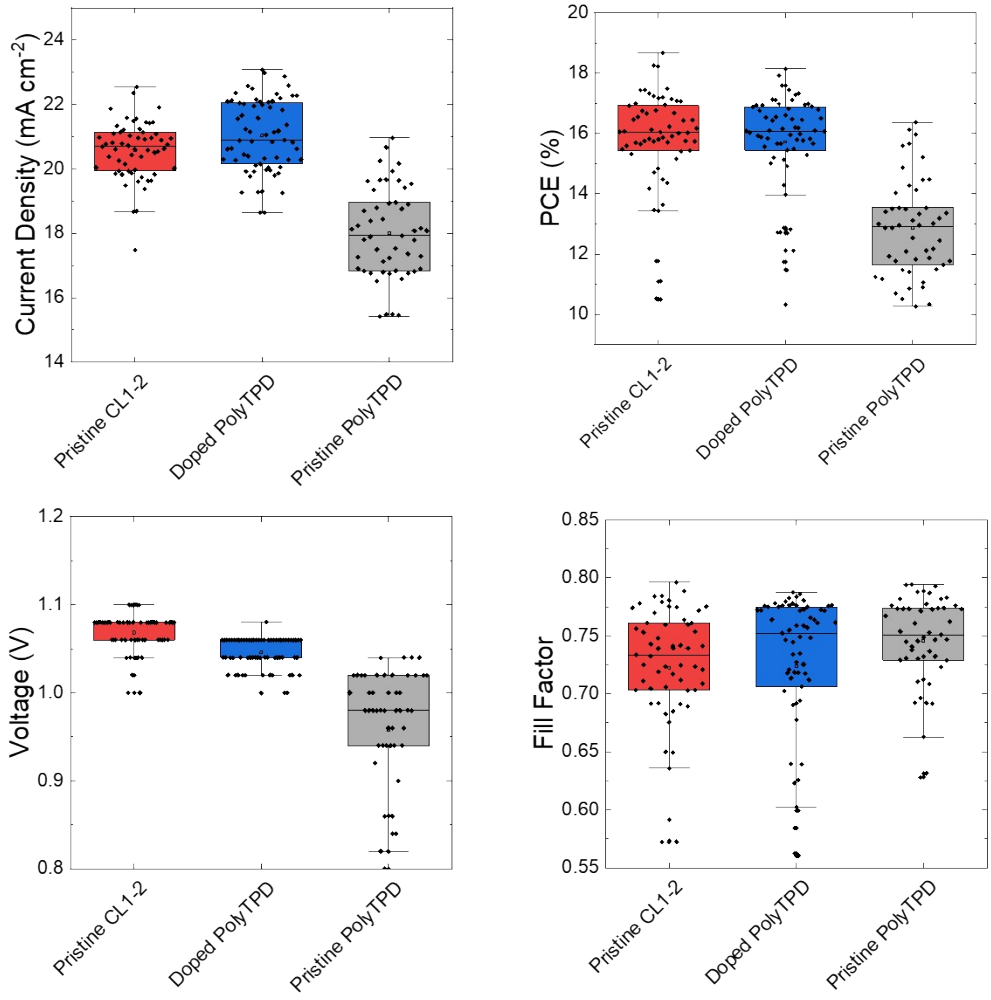

Fig. S7 Comparing the photovoltaic performance of FAMACs devices with pristine **CL1-2** and doped/undoped PolyTPD as HTM (1 mg mL^{-1}). Box-plot of devices prepared in 2 batches showing the comparison of the PV parameters (from J-V curves) of devices made using **CL1-2** and PolyTPD.

Table S1 Statistics for 48 individual FAMACs devices.

		J_{sc} (mA cm^{-2})	V_{OC} (V)	FF	PCE (%)
Pristine **CL1-2**	Average	20.6 ± 0.9	1.07 ± 0.02	0.72 ± 0.05	16 ± 2
	Maximum	22.6	1.10	0.80	18.7
Pristine PolyTPD	Average	18.0 ± 1.4	0.96 ± 0.08	0.72 ± 0.07	13 ± 2
	Maximum	21.0	1.04	0.79	16.4
Doped PolyTPD	Average	21.0 ± 1.1	1.05 ± 0.02	0.74 ± 0.04	16 ± 2
	Maximum	23.1	1.08	0.79	18.1

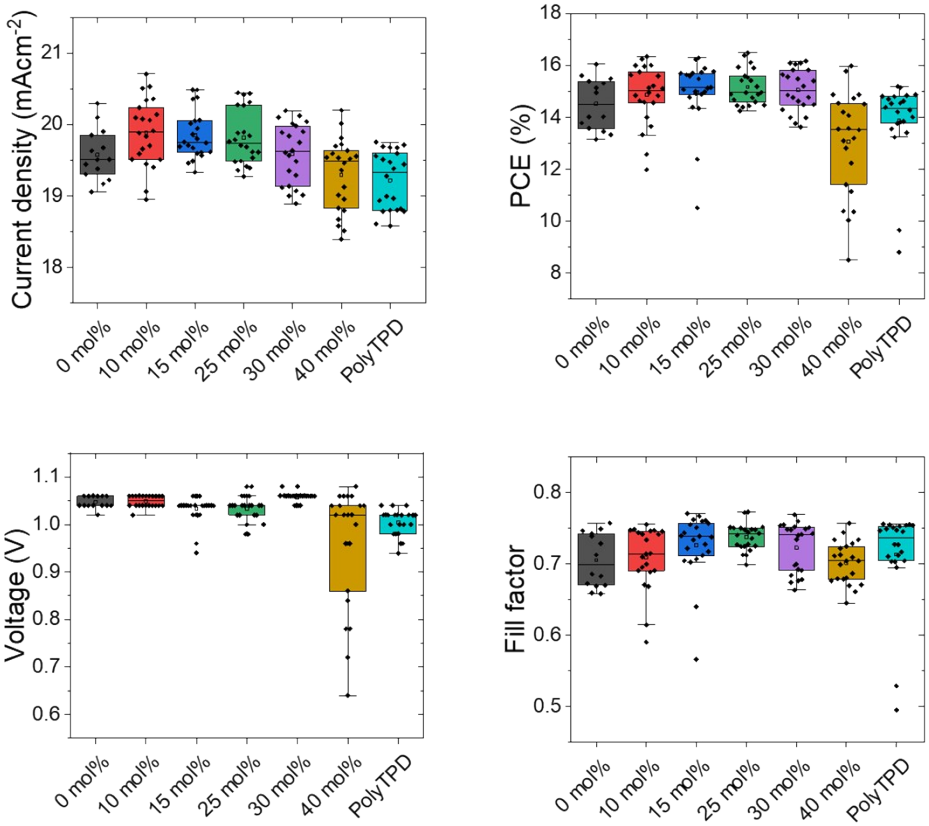

Fig. S8 Comparing the photovoltaic performance of FAMACs devices with different F_4-TCNQ concentration. Box-plot of 22 individual devices prepared in 2 batches showing the comparison of the PV parameters (from J-V curves) of devices comprising either PolyTPD or **CL1-2** at different dopant concentration. Note that these devices are not directly comparable to those in Figure S7 and Table S1 since the experiments shown here were conducted using unoptimized

HTM thicknesses (HTM concentration = 2 mg mL^{-1}), whereas those in Figure S7 are optimized HTM concentration = 1 mg mL^{-1}).

Table S2 Statistical for individual FAMACs devices made to optimize the dopant concentration when **CL1-2** is used as HTM (HTM concentration = 2 mg mL^{-1}).

		J_{sc} (mA cm^{-2})	V_{OC} (V)	FF	PCE (%)
CL1-2	Average	19.6 ± 0.4	1.05 ± 0.01	0.71 ± 0.04	15 ± 1
Undoped	Maximum	20.3	1.06	0.76	16.0
CL1-2	Average	19.8 ± 0.4	1.03 ± 0.03	0.74 ± 0.02	15.2 ± 0.7
25 mol% F_4-TCNQ	Maximum	20.4	1.08	0.77	16.5
CL1-2	Average	19.3 ± 0.5	1.0 ± 0.1	0.70 ± 0.03	13 ± 2
40 mol% F_4-TCNQ	Maximum	20.2	1.08	0.76	16.0
PolyTPD	Average	19.2 ± 0.4	1.00 ± 0.03	0.71 ± 0.07	14 ± 2
Doped	Maximum	19.8	1.04	0.76	15.2

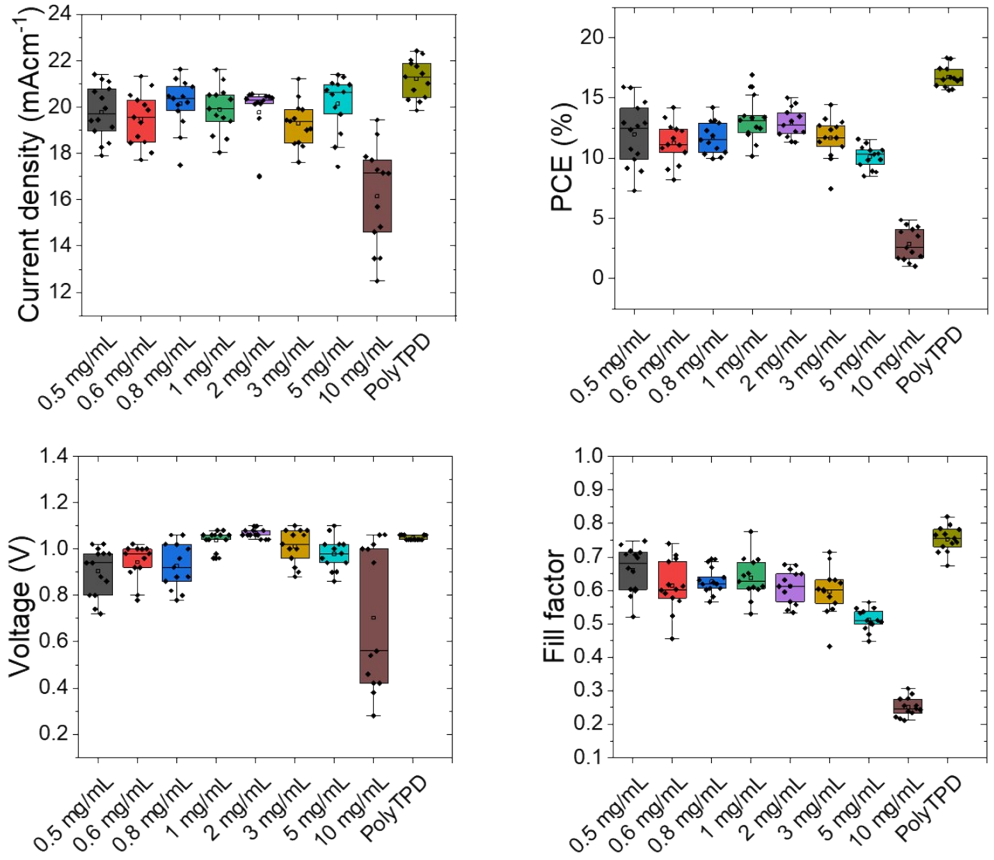

Fig. S9 Comparing the photovoltaic performance of FAMACs devices with different **P1-2** concentration used to cast 20 mol% doped **CL1-2** films. Box-plot of 14 individual devices prepared in 2 batches showing the comparison of the PV parameters (from J-V curves) of devices comprising either PolyTPD or **CL1-2** at different concentration as HTM.

Table S3 Statistics for 14 individual FAMACs devices made to optimize the concentration of **P1-2** used to cast 20 mol% doped **CL1-2** films.

		J_{sc} (mA cm^{-2})	V_{OC} (V)	FF	PCE (%)
0.5 mg mL^{-1} **P1-2**	Average	19.8 ± 1.2	0.90 ± 0.1	0.66 ± 0.07	12 ± 3
	Maximum	21.4	1.02	0.74	15.8
1 mg mL^{-1} **P1-2**	Average	19.9 ± 1.0	1.04 ± 0.04	0.64 ± 0.06	13 ± 2
	Maximum	21.6	1.08	0.78	16.9
3 mg mL^{-1} **P1-2**	Average	19.3 ± 0.9	1.01 ± 0.08	0.60 ± 0.07	12 ± 2
	Maximum	21.2	1.10	0.71	14.4
PolyTPD	Average	21.2 ± 0.9	1.05 ± 0.01	0.75 ± 0.04	16 ± 0.8
	Maximum	22.4	1.06	0.82	18.3

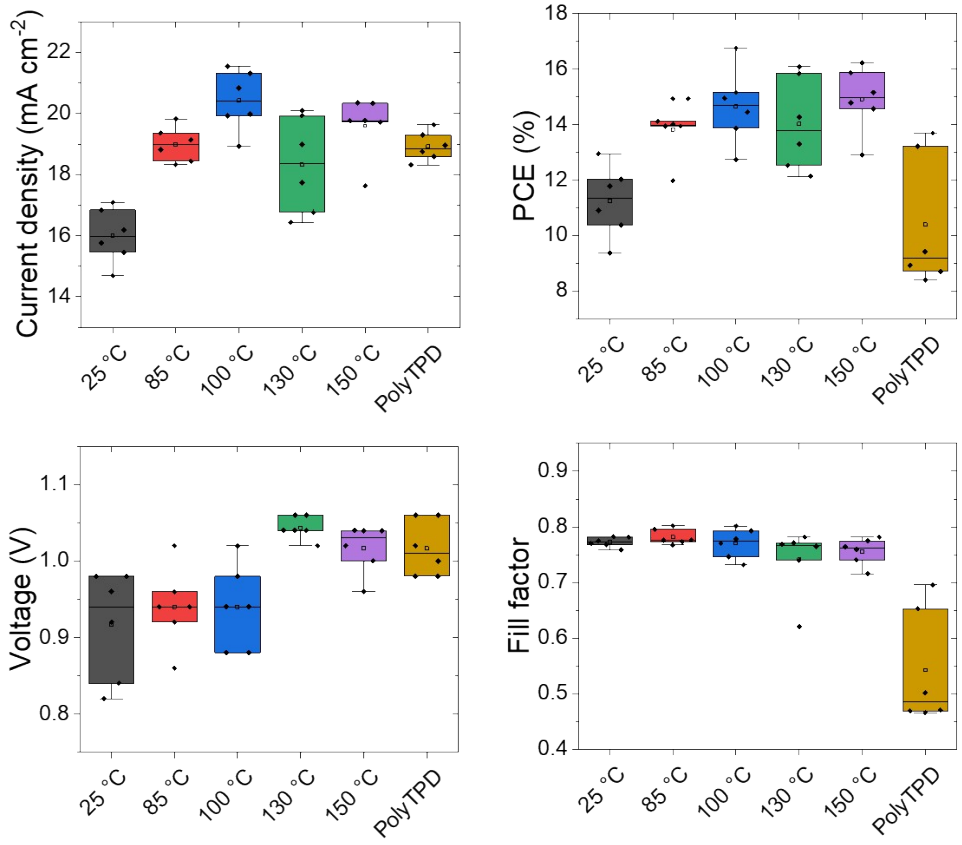

Fig. S10 Comparing the photovoltaic performance of FAMACs devices with different annealing temperature of **CL1-2**. Box-plot of 14 individual devices prepared in 1 batch showing the comparison of the PV parameters (from J-V curves) of devices comprising either PolyTPD or **CL1-2**, where **CL1-2** is annealed at different temperature.

Table S4 Overview statistical analysis of 14 individual FAMACs devices made to optimize the annealing temperature of **CL1-2**.

		J_{sc} (mA cm^{-2})	V_{OC} (V)	FF	PCE (%)
25 °C	Average	16.0 ± 0.9	0.92 ± 0.07	0.77 ± 0.01	11.2 ± 1.3
	Maximum	17.1	0.98	0.78	13.0
100 °C	Average	20.4 ± 1.0	0.94 ± 0.06	0.77 ± 0.03	14.7 ± 1.3
	Maximum	21.5	1.02	0.80	16.8
150 °C	Average	19.6 ± 1.0	1.02 ± 0.03	0.76 ± 0.02	14.9 ± 1.2
	Maximum	20.4	1.04	0.78	16.2
PolyTPD	Average	18.9 ± 0.5	1.02 ± 0.04	0.5 ± 0.1	10 ± 2
	Maximum	19.6	1.06	0.7	13.7

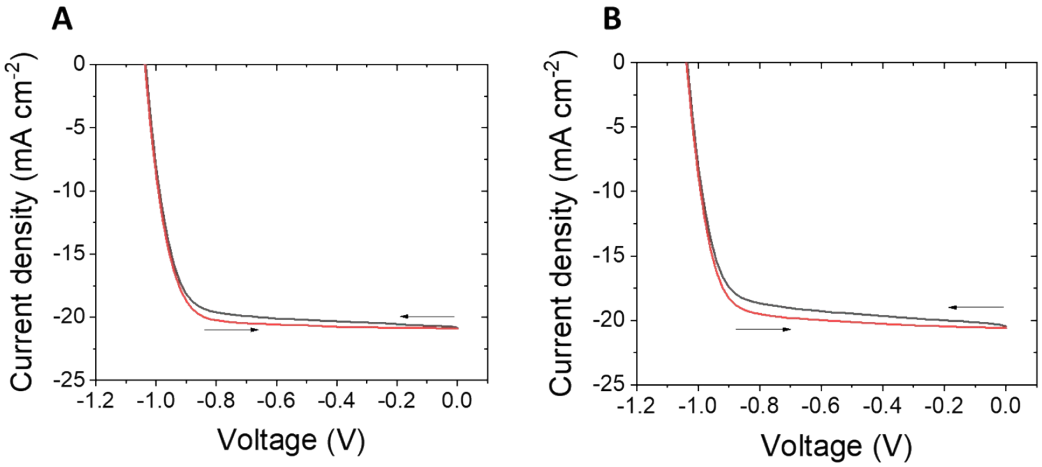

Fig. S11 Comparison of hysteresis in the J-V curves of FAMACs PSCs with (A) **CL1-2** and (B) PolyTPD HTMs.

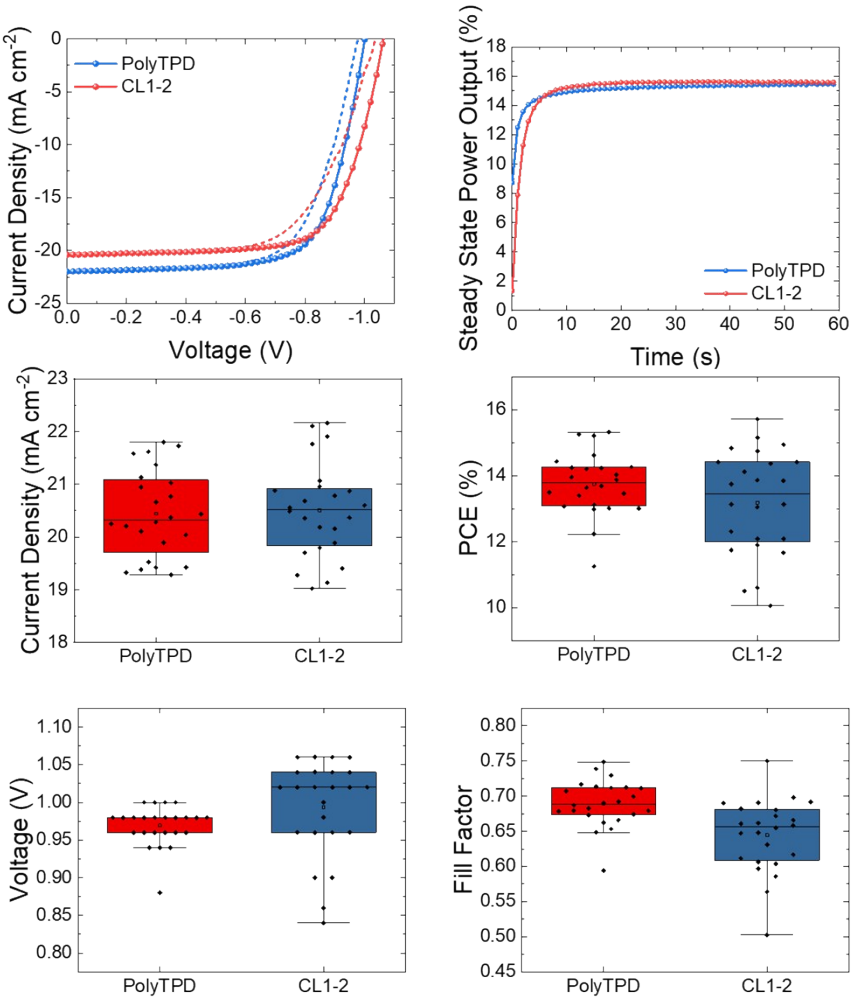

Fig. S12 Comparing the photovoltaic performance of FACs devices with different HTMs. Box-plot of 9 individual devices prepared in 1 batch showing the comparison of the PV parameters (from J-V curves) of devices comprising either PolyTPD or **CL1-2**.

Table S5 Statistics from 9 individual FACs devices.

		J_{sc} (mA cm^{-2})	V_{OC} (V)	FF	PCE (%)
CL1-2	Average	20.5 ± 0.9	0.99 ± 0.06	0.64 ± 0.03	13 ± 2
	Maximum	22.2	1.06	0.75	15.7
PolyTPD	Average	20.4 ± 0.8	0.97 ± 0.03	0.69 ± 0.03	13.8 ± 0.9
	Maximum	21.8	1.00	0.75	15.3

4. Additional data using more planar substrates

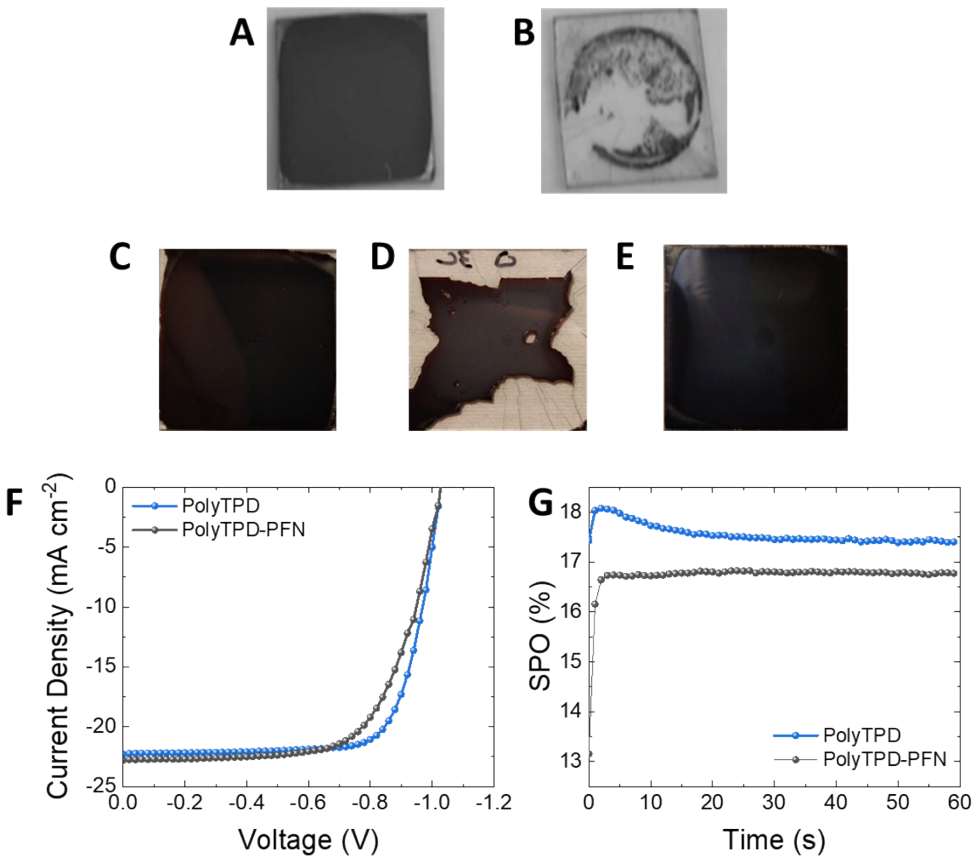

Fig. S13 A) Perovskite on Glass/**CL1-2 B)** Perovskite on Glass/PolyTPD **C)** Perovskite on ITO/**CL1-2 D)** Perovskite on ITO/PolyTPD **E)** Perovskite on ITO/PFN/PolyTPD on ITO. The perovskite is FACs. **F)** JV-curves of champion devices with and without PFN **G)** Stabilized power output of champion devices

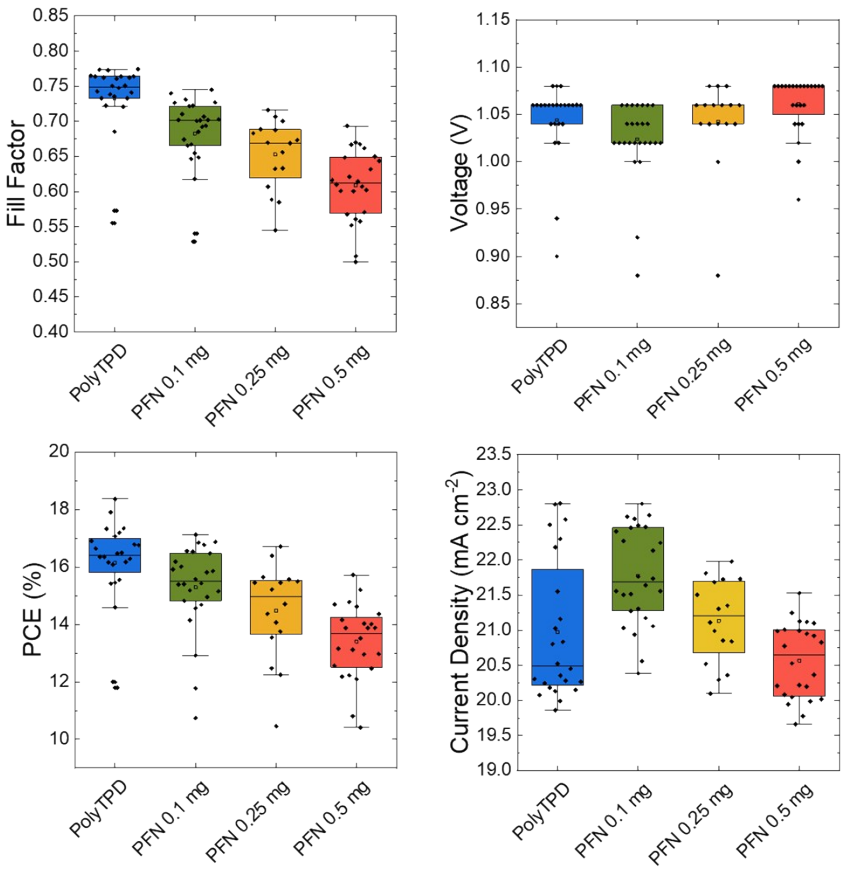

Fig. S14 Comparing the photovoltaic performance of FAMACs devices with different PFN concentration using ITO substrates. Box-plot of devices prepared in 1 batch showing the comparison of the PV parameters (from J-V curves) of devices comprising PolyTPD with increasing amount of PFN.

Table S6 Statistical for FAMACs devices made to optimize the PFN concentration in PolyTPD containing devices.

	n		J_{sc} (mA cm^{-2})	V_{OC} (V)	FF	PCE (%)
0.1 mg PFN	26	Average	21.0 ± 1.0	1.04 ± 0.04	0.73 ± 0.06	16 ± 2
		Maximum	22.8	1.08	0.77	18.4
0.25 mg PFN	16	Average	21.7 ± 0.7	1.02 ± 0.04	0.68 ± 0.05	15 ± 2
		Maximum	22.8	1.06	0.74	17.1
0.50 mg PFN	24	Average	21.1 ± 0.6	1.04 ± 0.05	0.65 ± 0.05	15 ± 2
		Maximum	22.0	1.08	0.72	16.7
PolyTPD	24	Average	20.6 ± 0.5	1.06 ± 0.03	0.61 ± 0.05	13.4 ± 1.3
		Maximum	21.5	1.08	0.69	15.7

Table S7 PLQE of the half device having the architecture FTO/HTM/FAMACs before and after 2 min photoirradiation with UV

	PLQE **t = 0 min**	**PLQE** **t = 2 min**
Doped CL1-2	0.256	0.208
Pristine CL1-2	0.218	0.190
Doped PolyTPD	0.277	0.085

4. Additional stability data

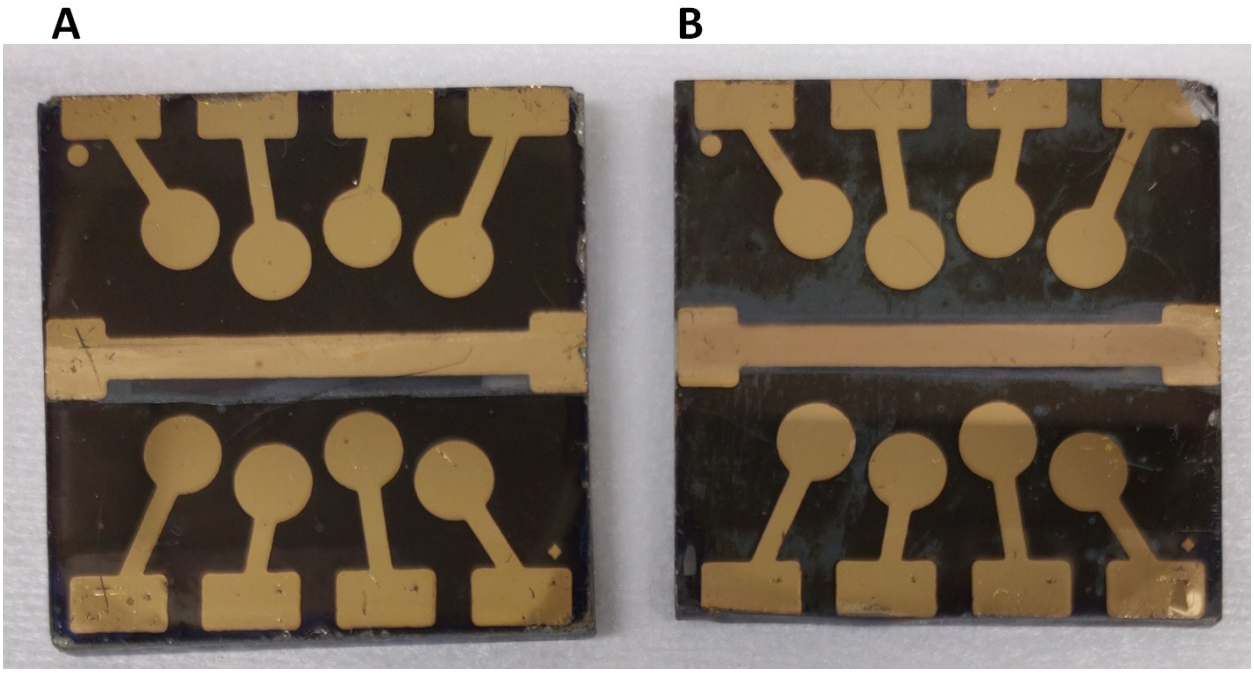

Fig. S15 CL1-2 (A) and PolyTPD (B) devices after aging experiment.

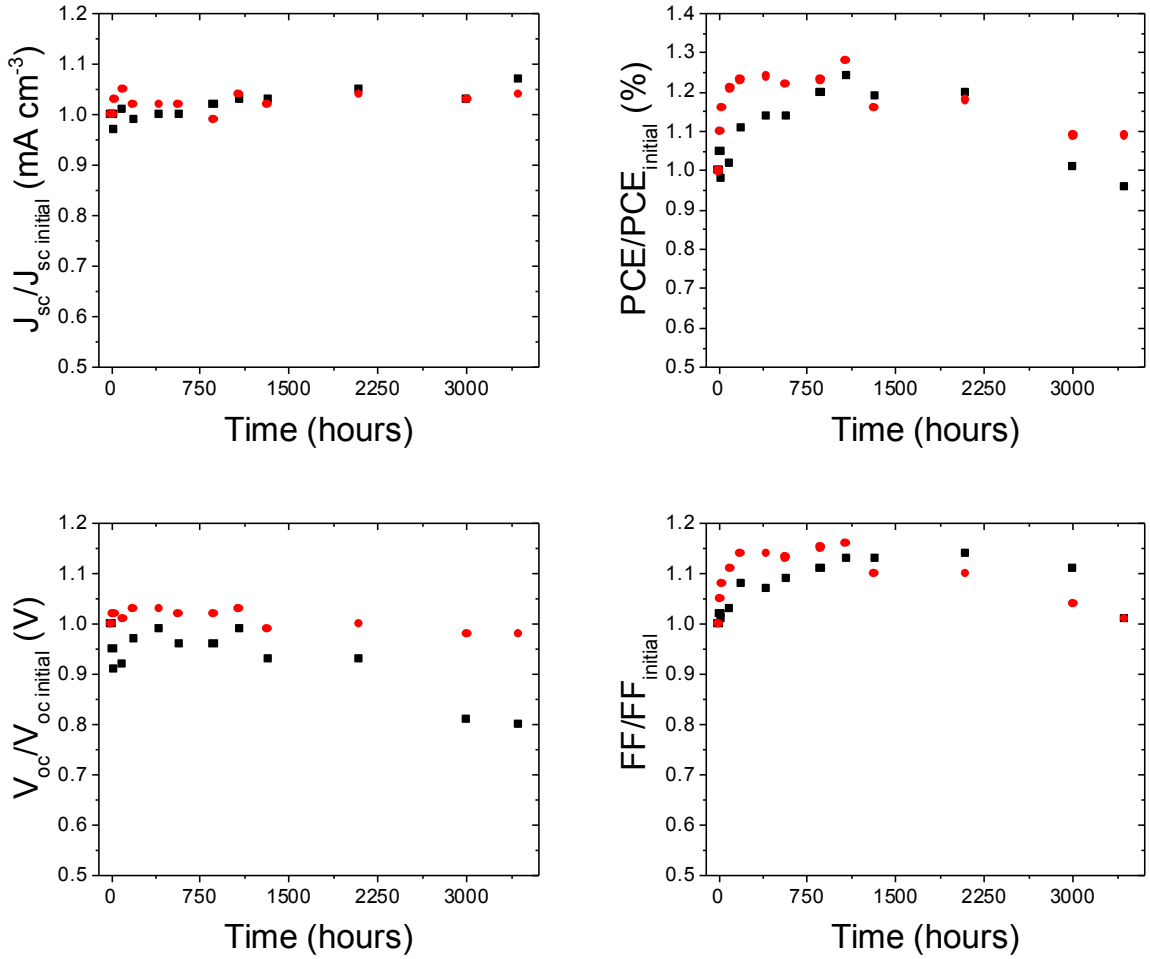

Fig. S16 Temporal evolution of photovoltaic parameters for $Cs_{0.05}(FA_{0.85}MA_{0.15})_{0.95}Pb(I_{0.9}Br_{0.1})_3$ PSCs devices at 85 °C in an oven inside a N_2-filled glovebox without encapsulation (from the same experiment as the stabilized power output data shown in Fig. 5A). The red circles correspond to devices with a polyTPD HTM, whereas the black squares are for **CL1-2** devices.

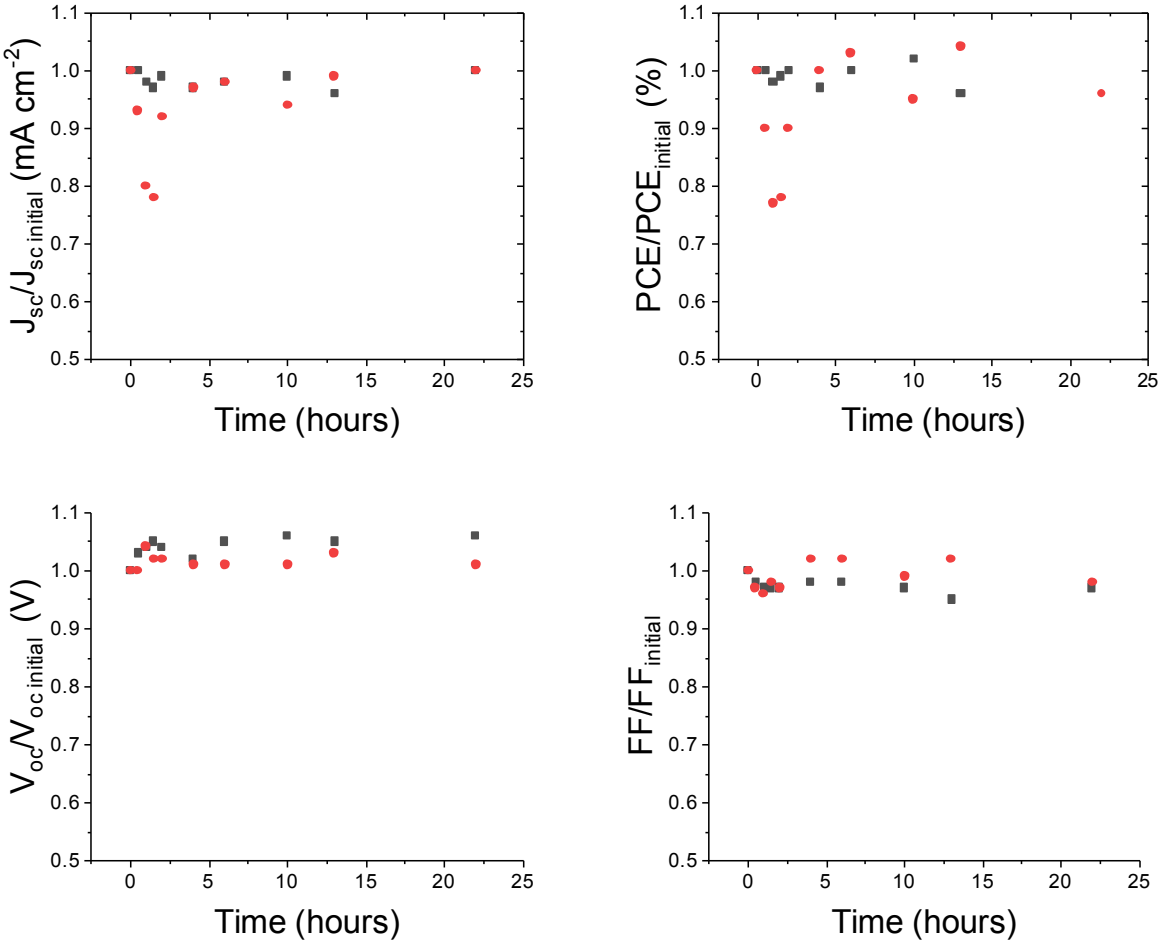

Fig. S17 Temporal evolution of PV parameters for $Cs_{0.05}(FA_{0.85}MA_{0.15})_{0.95}Pb(I_{0.9}Br_{0.1})_3$ PSCs devices under a UV LED light inside a N_2-filled glovebox without encapsulation (from the same experiment as the SPO and J data shown in Fig. 5B and C; red circles = polyTPD HTM; black squares = **CL1-2**).

References for ESI

1. Y.-D. Zhang, R. D. Hreha, G. E. Jabbour, B. Kippelen, N. Peyghambarian and S. R. Marder, *J. Mater. Chem.*, 2002, **12**, 1703-1708.
2. S. D. Stranks, G. E. Eperon, G. Grancini, C. Menelaou, M. J. P. Alcocer, T. Leijtens, L. M. Herz, A. Petrozza and H. J. Snaith, *Science*, 2013, **342**, 341.
3. G. E. Eperon, S. D. Stranks, C. Menelaou, M. B. Johnston, L. M. Herz and H. J. Snaith, *Energ. Environ. Sci.*, 2014, **7**, 982-988.
4. D. W. de Quilettes, S. M. Vorpahl, S. D. Stranks, H. Nagaoka, G. E. Eperon, M. E. Ziffer, H. J. Snaith and D. S. Ginger, *Science*, 2015, **348**, 683.
5. D. W. deQuilettes, S. Koch, S. Burke, R. K. Paranji, A. J. Shropshire, M. E. Ziffer and D. S. Ginger, *ACS Energy Lett.*, 2016, **1**, 438-444.
6. N. K. Noel, S. N. Habisreutinger, B. Wenger, M. T. Klug, M. T. Hörantner, M. B. Johnston, R. J. Nicholas, D. T. Moore and H. Snaith, *Energy Environ. Sci.* 2017, **10**, 145-152.
7. Y. Shao, Z. Xiao, C. Bi, Y. Yuan and J. Huang, *Nat. Commun.*, 2014, **5**, 5784.
8. H. Li, L. Tao, F. Huang, Q. Sun, X. Zhao, J. Han, Y. Shen and M. Wang, *ACS Appl. Mater. Interfaces*, 2017, **9**, 38967-38976.
9. D. Bi, C. Yi, J. Luo, J.-D. Décoppet, F. Zhang, Shaik M. Zakeeruddin, X. Li, A. Hagfeldt and M. Grätzel, *Nat. Energy*, 2016, **1**, 16142.